ARTICLE

Decay Dynamics of N, N-Dimethylthioacetamide in $S_3(\pi\pi^*)$ State

Xiao Chen[a], Jia-dan Xue[a], Xu-ming Zheng[a,b,c*]

a. Department of Chemistry, Zhejiang Sci-Tech University, Hangzhou 310018, China
b. Key Laboratory of Advanced Textiles Materials and Manufacture Technology of the Ministry of Education, Zhejiang Sci-Tech University, Hangzhou 310018, China
c. Engineering Research Center for Eco-dyeing and Finishing of Textiles of the Ministry of Education, Zhejiang Sci-Tech University, Hangzhou 310018, China

(Dated: Received on September 11, 2014; Accepted on October 30, 2014)

The decay dynamics of N, N-dimethylthioacetamide after excitation to the $S_3(\pi\pi^*)$ state was studied by using the resonance Raman spectroscopy and complete active space self-consistent field method calculations. The UV-absorption and vibrational spectra were assigned. The A-band resonance Raman spectra were obtained in acetonitrile, methanol and water with the laser excitation wavelengths in resonance with the first intense absorption band to probe the Franck-Condon region structural dynamics. The CASSCF calculations were carried out to determine the excitation energies and optimized structures of the lower-lying singlet states and conical intersection point. The A-band structural dynamics and the corresponding decay mechanism were obtained by the analysis of the resonance Raman intensity pattern and the CASSCF calculated structural parameters. The major decay channel of $S_{3,FC}(\pi\pi^*)\rightarrow S_3(\pi\pi^*)/S_1(n\pi^*)\rightarrow S_1(n\pi^*)$ is proposed.

Key words: N, N-Dimethylthioacetamide, Structural dynamics, Decay dynamics, Resonance Raman spectrum, CASSCF calculation, Conical intersection

I. INTRODUCTION

Thioacetamide is a derivative of acetamide, in which the carbonyl oxygen atom is replaced by sulfur. The photophysics and photochemistry of thiocarbonyls were reviewed by Maciejewski and Steer [1]. Previous studies have shown that the thione forms of small thioamides are much more stable than the thiol tautomers in the ground electronic state [2−4]. The calculated energy difference between the thione and thiol forms of thioacetamide is 39.1 kJ/mol, which precludes thermal population of the thiol form of thioacetamide in the ground electronic state due to large transition energy barrier [5]. UV-induced intramolecular proton-transfer reactions leading to conversion of a thione form to the corresponding thiol form were observed for a number of matrix-isolated thioamides [6−10]. In some heterocyclic compounds, UV excitation induces proton transfer to exocyclic sulfur atom from a nitrogen atom placed in a ring in an α position with respect to the C=S group. It should be pointed out that this type of unimolecular proton-transfer reactions is fundamentally different from the classic UV-induced proton-transfer reactions known as excited state intramolecular proton-transfer (ESIPT) processes [11]. The ESIPT-type proton transfer requires an intramolecular hydrogen bond, along which proton is moved in the excited state. This is neither fulfilled for the heterocyclic compounds studied nor for thioacetamide.

Resonance Raman spectroscopy has proven to be a powerful tool in the understanding of various processes such as vibronic-coupling [12−14], excited state proton-transfer (ESPT) or hydrogen atom detachment and attachment reactions [15−18], and photodissociation [19, 20].

In the present work, a resonance Raman spectroscopy and CASSCF calculation of the excited state decay dynamics of N, N-dimethylthioacetamide (DMTAA) were carried out to examine how the methyl substitution changes the short-time structural dynamics and the subsequent decay mechanism of thioacetamide and its derivatives.

II. EXPERIMENTAL AND COMPUTATIONAL METHODS

Thioacetamide was purchased from J&K Scientific Ltd. Concentrations of approximately 2.0−5.0 mmol/L acetamide were prepared using HPLC grade solvents of acetonitrile (99.9%, Tedia, USA), methanol (99.9%, Spectrum, USA) and de-ionized water. The Fourier transform (FT)-Raman and FT-IR spectra were obtained using FT-Raman (Thermo Nicolet 960, Thermo Fisher Nicolet, USA) and FT-IR (Thermo Nicolet

*Author to whom correspondence should be addressed. E-mail: zxm@zstu.edu.cn, Tel.: +86-571-86843699

avatar 370, Thermo Fisher Nicolet, USA) spectrometers with 2 cm^{-1} resolution. The UV absorption spectrum was measured using UV/visible spectrometer (UV-2501PC, Shimadzu, Japan).

The resonance Raman experimental method and apparatus have been described previously [19], only a short description is given here. The harmonics of a nanosecond Nd:YAG laser and their hydrogen Raman shifted laser lines were employed to generate the 309.1, 282.4, 266.0, 252.7, 245.9, and 239.5 nm excitation wavelengths which were utilized in the resonance Raman experiments. The excitation laser beam used a ∼100 μJ pulse energy loosely focused to a 0.5−1.0 mm diameter spot size onto a flowing liquid stream of sample. A backscattering geometry was employed for collection of the Raman scattered light by reflective optics that imaged the light through a polarizer and entrance slit of a 0.5 m spectrograph and the grating of the spectrograph dispersed the light onto a liquid nitrogen cooled CCD mounted on the exit of the spectrograph. The Raman shifts of the resonance Raman spectra were calibrated with the known vibrational frequencies of solvent Raman bands (cyclohexane, acetonitrile and methanol). To fully subtract the solvent Raman bands from the resonance Raman spectra of the sample solutions, the pure solvent Raman spectrum at certain excitation wavelength is scaled by a proper factor so that the intensities of the scaled solvent Raman bands match those of the corresponding bands in the sample resonance Raman spectrum at the same excitation wavelength. Sections of the resonance Raman spectra were fit to a baseline plus a sum of Lorentzian bands to determine the integrated areas of the Raman bands of interest. The resonance Raman spectra have been intensity-corrected [20] for the wavelength dependence of the sample's absorbance in backscattering geometry [21] and for the spectrograph throughput and detector quantum efficiency [22]. The spectral resolution is about 6 cm^{-1} for the 217.8 nm resonance Raman spectrum, and 3 cm^{-1} for the 299.1 nm one.

The geometry structure optimization and vibrational frequency computation were done using the B3LYP/6-311++G(d,p) level of theory. The $S_0 \rightarrow S_n$ vertical transition energies were estimated at B3LYP-TD/6-311++G(d,p) levels of theory employing a self-consistent reaction field (SCRF), polarized continuum overlapping spheres model (PCM). The complete active space self-consistent field (CASSCF) theory was used to study the excited state decay mechanism of PITC. The conical intersection and intersystem crossing points between two electronic excited states were computed at CASSCF(6,5)/6-31G(d) level of theory. Seven active orbitals were used for the CASSCF calculations. An active space with 6 electrons in 5 orbitals is referred to as CASSCF(6,5) hereafter. All of the quantum mechanical calculations were done using the Gaussian 03 program [23].

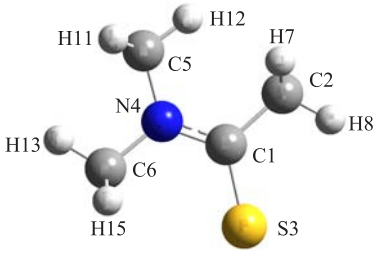

FIG. 1 The schematic diagram of the geometry structure of DMTAA.

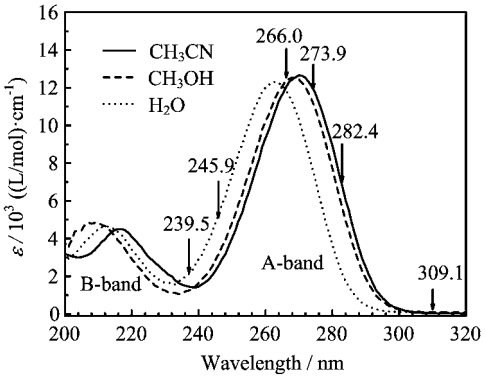

FIG. 2 UV spectra of DMTAA in acetonitrile, methanol, and water with the excitation wavelengths used for the resonance Raman experiment indicated above the curves.

III. RESULTS AND DISCUSSION

A. UV spectra

Figure 1 shows the schematic diagram of the geometry structure and Fig.2 shows the UV spectra of DMTAA in acetonitrile, methanol and water with the excitation wavelengths used for the resonance Raman experiment indicated above the curves. In acetronitrile, the experimental UV spectrum displays two bands in >200 nm spectral region with λ_{max} being at 270 nm (f=0.2779) and 217 nm (f=0.1407) respectively, and they are termed as A-band and B-band. The molecular coefficient, ε, measured for the A-band absorption in acetonitrile, methanol, and water are 1.27×10^4 (L/mol)·cm^{-1} (λ_{max}=270 nm), 1.25×10^4 (L/mol)·cm^{-1} (λ_{max}= 268 nm), and 1.23×10^4 (L/mol)·cm^{-1} (λ_{max}=263 nm), respectively. The blue-shifts of the A-band absorption are noticeably observed as solvent goes from nonpolar to polar.

Table I lists the B3LYP-TD/6-311++G(d,p) computed electronic transition energies and oscillator strengths of DMTAA with the experimental data taken in acetonitrile for comparison. Figure 3 shows the molecular orbitals associated with the electronic transitions of DMTAA. The orbitals 27 and 28 are π bonding orbital (π_{H-1}) and non-bonding orbital (n_H), and their

DOI:10.1063/1674-0068/28/cjcp1409152

TABLE I TD-B3LYP/6-311++G(d,p) computed electronic transition energies E, and oscillator strengths f of DMTAA. The experimental data are taken in acetonitrile.

State	Orbitals	Character	E/nm (eV)		f	
			Calc.	Expt.	Calc.	Expt.
$S_1(A'')$	28→29(0.71)	$n_H \rightarrow \pi_L^*$	339 (3.66)		0.0002	
$S_2(A')$	28→30(0.67)/27→29(−0.14)/28 →32(−0.14)	$n_H \rightarrow Ryd_1/\pi_{H-1} \rightarrow \pi_L^*/n_H \rightarrow Ryd_3$	246 (5.04)	270 (A-band)	0.0637	
$S_3(A')$	27→29(0.67)/28→30(0.13)	$\pi_{H-1} \rightarrow \pi_L^*/n_H \rightarrow Ryd_1$	245 (5.06)	270 (A-band)	0.3355	0.2779
$S_4(A'')$	27→30(0.70)	$\pi_{H-1} \rightarrow Ryd_1$	228 (5.45)	217 (B-band)	0.0588	0.1407
$S_5(A')$	28→32(0.66)/28→30(0.15)/28 →35(0.11)/28→36(0.14)	$n_H \rightarrow Ryd_3/n_H \rightarrow Ryd_1/n_H \rightarrow Ryd_6/n_H \rightarrow Ryd_7$	218 (5.68)	217 (B-band)	0.0392	
$S_6(A')$	28→31(0.68)/28→34(0.14)	$n_H \rightarrow Ryd_2/n_H \rightarrow Ryd_5$	216 (5.74)		0.0079	

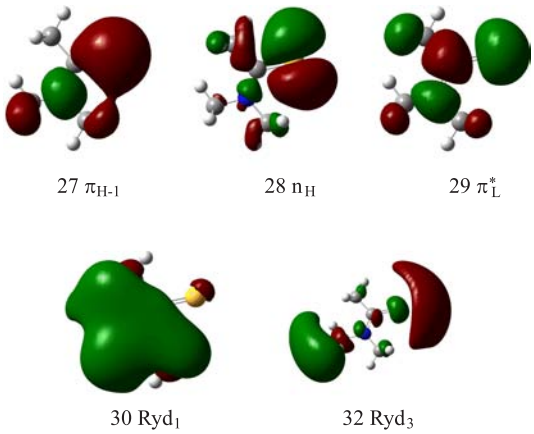

FIG. 3 TD-B3LYP/6-311++G(d,p) computed molecular orbitals associated with the electronic transitions of DMTAA.

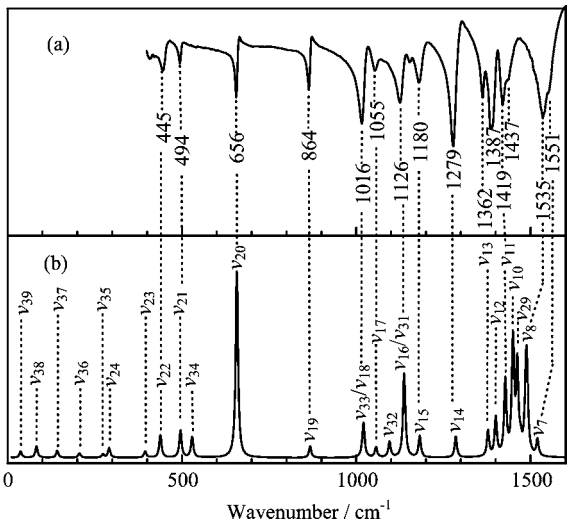

FIG. 4 (a) Experimental FT-IR spectrum in neat liquid of water in comparison with (b) the calculated non-resonance Raman spectrum. The calculated frequencies are scaled linearly to those observed in the FT-IR spectrum.

electronic densities are localized mostly on N=C=S and C=S moieties respectively, while the orbital 29 is π^* anti-bonding orbital (π_L^*) with the electronic density being localized mostly on N=C=S moiety. Orbitals 30 and 31 are two diffused Rydberg orbitals with major amplitude across nine hydrogen atoms of three methyl group. The calculated UV spectrum displays four electronic excited states (S_2, S_3, S_4, and S_5) that have moderate to large oscillator strengths. Due to the limited spectral resolution, the experimental A-band absorption can reasonably correlate to the $S_0 \rightarrow S_2$ transition at 246 nm (f=0.0637) and the $S_0 \rightarrow S_3$ transition at 245 nm (f=0.3355). Thus the A-band absorption is assigned as the combined major $\pi_{H-1} \rightarrow \pi_L^*(0.67)$ transition and the moderate $n_H \rightarrow Ryd_1(0.67)$ transition based on the calculated orbital transitions and the corresponding oscillator strengths. Similarly, the B-band absorption can be assigned as the major $\pi_{H-1} \rightarrow Ryd_1(0.70)$ transition and $n_H \rightarrow Ryd_3(0.66)$ transition. It is worthy to point out that five diffuse Rydberg orbitals are also involved in the A- and B-band absorption, and they are expected to play important roles in the excited state dynamics.

B. Vibrational assignment

There has been no reports for the vibrational assignment of DMTAA. To make the vibrational assignments, the FT-IR spectrum and the A-band resonance Raman spectra in different solvents are measured and the density functional theory calculation is carried out. Due to the burning of the sample, the measurements of the FT-Raman spectra in neat solid, in different solvents and at lower temperature are unsuccessful. Figure 4 shows the FT-IR spectrum in neat liquid in comparison with the calculated Raman spectra. Table II presents the B3LYP/6-311++G(d,p) calculated non-resonance Raman and the experimentally (FT-IR and A-band resonance Raman) observed vibrational frequencies and normal mode descriptions of DMTAA. The tentative correlation between the experimental frequencies and the calculated ones are done as follows.

In 0−299 cm^{-1} spectral region, no experimental

DOI:10.1063/1674-0068/28/cjcp1409152

TABLE II B3LYP/6-311++G(d,p) calculated and FT-IR observed vibrational frequencies and normal mode descriptions of DMTAA. Experiment data are from resonance Raman at 266.0 nm.

	Calc./cm^{-1}		Expt.[a]/cm^{-1}			FT-IR	Description	PED/%
	R/IR	Scaled	H_2O	CH_3CN	CH_3OH			
A′								
ν_1	3181(41/7.5)	3122					C5H12 stretch/H10C5H11 sym stretch	50/17
ν_2	3161(34/2.6)	3102					C2H8 stretch/H7C2H9 sym stretch	50/19
ν_3	3126(68/18)	3068					C6H13 stretch/H14C6H15 sym stretch	42/33
ν_4	3039(205/35)	2983					H14C6H15 sym stretch/C6H13 stretch sym	55/21
ν_5	3019(255/34)	2963					H7C2H9 sym stretch/C2H8 stretch sym	61/11
ν_6	3017(149/39)	2961					H10C5H11 sym stretch sym	55
ν_7	1543(2.6/163)	1520	1543(m)	1544(m)	1555(s)	1551(m)	H10C5H11 scissor/C1N4 stretch/ N4C6H13 bend	20/13/13
ν_8	1512(13/11)	1489	1523(m)	1520(m)	1515(w)	1535(vs)	H10C5H11 scissor/C5H12 bend	31/11
ν_9	1494(1.6/4.7)	1472					H14C6H15 scissor/H10C5H11 wag	52/14
ν_{10}	1471(11/13)	1449				1437(m)	C2-methyl deforemation/C6-methyl umbrella	38/20
ν_{11}	1449(11/3.5)	1428				1419(s)	C5/C6-methyl umbrella	45/29
ν_{12}	1421(5.7/152)	1400	1393(m)	1398(m)	1401(s)	1387(vs)	C6-methyl umbrella/H10C5H11 scissor/ C1N4 stretch	34/20/18
ν_{13}	1398(3.8/15)	1378	1369(w)	1366(w)	1365(w)	1362(s)	C2H3 umbrella	54
ν_{14}	1303(3.1/106)	1285	1283(m)	1280(m)	1275(m)	1279(vs)	C1N4C5/C1N4C6 bend/H7C2H9/ H14C6H15 wag	27/19/13/10
ν_{15}	1198(3.1/68)	1182	1181(w)	1178(w)	1173(w)	1180(m)	C2/C5/C6-methyl wag/C1N4 stretch	25/19/26/12
ν_{16}	1152(12/11)	1137	1132(s)	1132(s)	1127(s)	1126(s)	C1C2 stretch/C1S3 bend/C5-methyl wag	25/13/20
ν_{17}	1069(1.4/12)	1056	1073(w)	1079(w)	1082(w)	1055(w)	C6-/C5-methyl bend	48/36
ν_{18}	1033(4.4/57)	1021	1015(w)			1016(vs)	C2-/C5-methyl bend	42/22
ν_{19}	876(1.5/7.1)	868	866(m)	863(m)	862(m)	864(s)	C5N4C6 sym stretch+C2-methyl/ C1S3 bend	30/30/14
ν_{20}	661(24/3.1)	657	656(vs)	657(vs)	652(vs)	656(s)	C5N4C6 sym stretch/C1C2/C1S3/C1N4 stretch sym	30/26/15/10
ν_{21}	496(3.3/4.0)	496	495			494(m)	C1N4C6 scissor	100
ν_{22}	437(2.7/4.6)	438	446			445(m)	C5N4C6 scissor	84
ν_{23}	393(0.7/0.9)	395	399				C_2-methy bend	62
ν_{24}	287(1.1/23)	292					C5N7C6 rock/C1S3 bend	46/27
A″								
ν_{25}	3097(39/12)	3040					H14C6H15 asym stretch asym	71
ν_{26}	3072(65/11)	3015					H7C2H9 asym stretch asym	75
ν_{27}	3061(134/28)	3004					H10C5H11 asym stretch asym	69
ν_{28}	1509(6.5/0.3)	1487					C5/C2-methy twist	48/42
ν_{29}	1484(14/12)	1462					C2/C5-methyl twist	47/46
ν_{30}	1472(6.9/17)	1450					C6-methyl twist	80
ν_{31}	1156(0.3/0.7)	1141				1153(w)	C5/C6-methyl twist	42/41
ν_{32}	1109(2.2/0.0)	1095					C6/C5-methyl twist	48/45
ν_{33}	1029(0.6/0.0)	1017					C2-methyl twist	74
ν_{34}	530(2.5/0.3)	529	539				C1 out-of-plane bend/C2-methyl twist	53/18
ν_{35}	269(0.4/3.1)	274					N4 out-of-plane bend/C2/C5/ C6-methy twist	40/14/23/23
ν_{36}	200(0.5/1.0)	206					C2-methyl torsion	66
ν_{37}	135(0.8/0.7)	143					C6-methyl torsion	62
ν_{38}	74(1.3/0.0)	83					C2/C5/C6-methyl torsion	21/49/23
ν_{39}	27(0.7/0.0)	37					C6-/C5-methyl torsion	48/37

[a] Scaled=10.8+0.978×B3LYP/6-311++G(d,p) calculated.

DOI:10.1063/1674-0068/28/cjcp1409152

bands are observed so that no correlation between the experimental and the calculated ones can be made. In 300−1300 cm^{-1} spectral region, the twelve observed bands at 399, 446, 495, 539, 661, 876, 1015, 1073, 1132, 1181, and 1283 cm^{-1} in the 309.1 nm resonance Raman spectra and/or at –, 445, 494, –, 656, 864, 1016, 1055, 1126, 1153, 1180, –, and 1279 cm^{-1} in the FT-IR spectrum correlate well with the (spectroscopically scaled) calculated bands at 395, 438, 496, 529, 657, 868, 1021/1017, 1056, 1137, 1141, 1182, 1285 cm^{-1} and they are respectively assigned to ν_{23}, ν_{22}, ν_{21}, ν_{34}, ν_{20}, ν_{19}, ν_{18}, ν_{17}, ν_{16}, ν_{31}, ν_{15}, and ν_{14}.

In 1300−1500 cm^{-1} spectral region, the experimental spectrum displays two bands at 1369 and 1393 cm^{-1} in the 309.1 nm resonance Raman spectrum and four bands at 1362, 1387, 1419, 1437 cm^{-1} in the FT-IR spectrum, and they correlate well with the (spectroscopically scaled) calculated bands at 1378, 1400, 1428, and 1449 cm^{-1}, and are assigned as ν_{13}, ν_{12}, ν_{11}, ν_{10}. The (spectroscopically scaled) calculated band at 1472 cm^{-1} (or the band at 1494 cm^{-1} without scaling) is not observed. In 1500−1600 cm^{-1} region, two observed bands at 1523, 1543 cm^{-1} in the 309.1 nm resonance Raman spectrum and at 1535, 1551 cm^{-1} in FT-IR spectrum correlate with the calculated bands at 1512, 1543 cm^{-1}, and they are assigned as ν_8, ν_7.

Figure 5 shows the A-band resonance Raman spectra of DMTAA in three solvents. According to Fig.2 and Table I, the 309.1 nm resonance Raman spectrum is mostly the pre-resonance Raman spectrum of the A-band absorption so that it provides important information on the fundamental vibrational modes that are active in the A-band resonance Raman spectra in 0−1600 cm^{-1} spectral region. This spectrum may also provide the information on the vibronic-coupling or state-mixing among S_3, S_2, and S_1. Similarly, the 239.5 nm resonance Raman spectrum may also give the information on the vibronic-coupling or state-mixing among S_3 and the higher-lying states.

Figure 6 shows the expanded view of the 273.9 and 266.0 nm resonance Raman spectra in acetonitrile and water respectively. Most of the A-band resonance Raman intensities of DMTAA in acetonitrile and water can be assigned to the fundamentals, overtones and combination bands of about ten Franck-Condon modes: ν_7, ν_8, ν_{12}, ν_{13}, ν_{14}, ν_{15}, ν_{16}, ν_{17}, ν_{19}, ν_{20}.

To insight into the excited state structural dynamics of DMTAA buried behind the different resonance Raman intensity pattern, we recall first the relation between the Raman band intensity I_i and the normal mode displacement Δ_i or vibrational reorganization energy λ_i for a certain fundamental mode ν_i with frequency ω_i: $I_i=k{\omega_i}^2{\Delta_i}^2$, or $\lambda_i=kI_i/2\omega_i$, where k is a constant. Table III lists Δ_i and λ_i calculated for the Franck-Condon active modes from the A-band resonance Raman spectra in acetonitrile and water.

According to $I_i=k{\omega_i}^2{\Delta_i}^2$, if two fundamental modes have the same normal mode displacements, the mode that has higher frequency will possess larger Raman intensity. Alternatively if two modes have the same Raman intensities, the mode that has higher frequency will undergo smaller normal mode displacement. Table III shows that the largest relative normal mode displacement or vibrational reorganizational

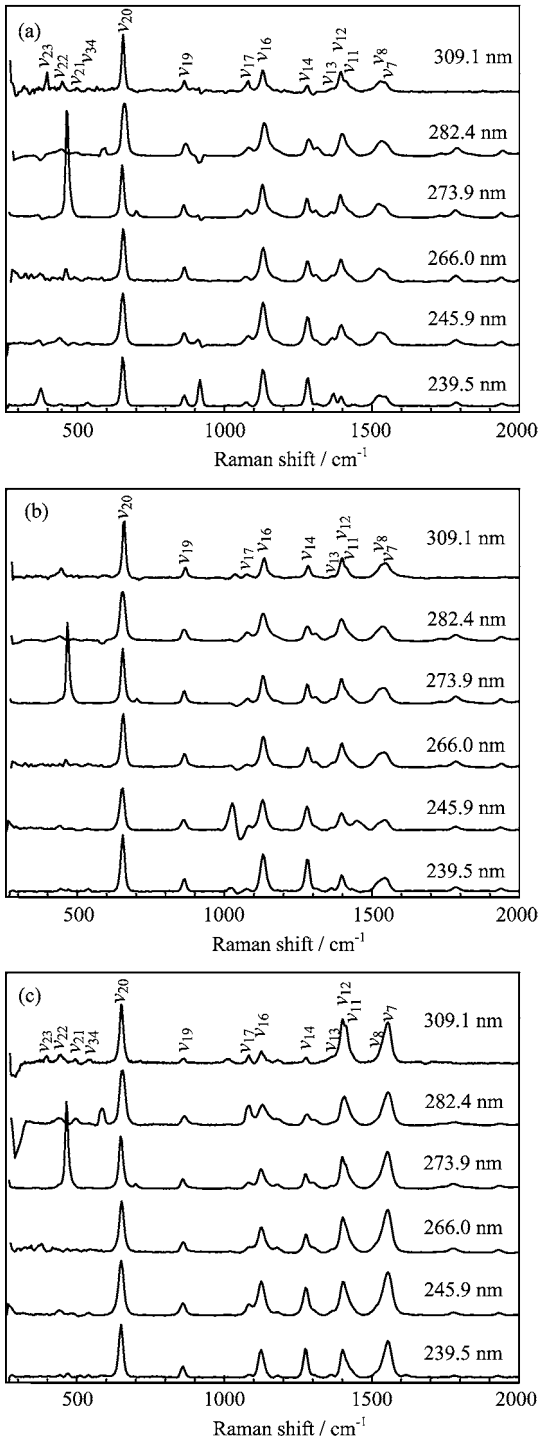

FIG. 5 Overall view of the A-band resonance Raman spectra of DMTAA in (a) acetonitrile, (b) methanol, (c) water.

DOI:10.1063/1674-0068/28/cjcp1409152

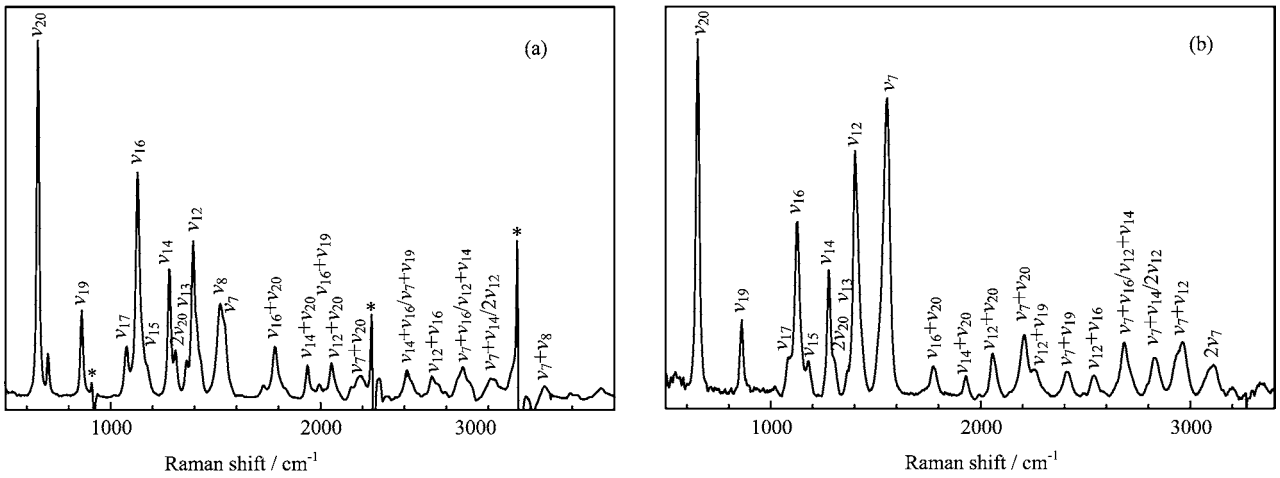

FIG. 6 Expanded view of (a) the 273.9 nm in acetonitrile and (b) the 266.0 nm one in water for the resonance Raman spectra of DMTAA. The peaks labeled with star.

TABLE III Experimentally measured absolute Raman cross section σ_R (10^{-8} Å^2/molecule), and the relative normal mode displacement $\Delta_i/\Delta(\nu_{20})$ and relative vibrational reorganizational energy $\lambda_i/\lambda(\nu_{20})$ for the Franck-Condon active modes in water and acetonitrile.

Raman peaks	Raman shift/cm^{-1}	273.9 nm in acetonitrile			266.0 nm in water		
		σ_R	$\Delta_i/\Delta(\nu_{20})$	$\lambda_i/\lambda(\nu_{20})=I_i/2\omega_i$	σ_R	$\Delta_i/\Delta(\nu_{20})$	$\lambda_i/\lambda(\nu_{20})=I_i/2\omega_i$
ν_{20}	652	1.74	1.00	1.00	2.00	1.00	1.00
ν_{19}	862	0.42	0.37	0.18	0.49	0.37	0.19
ν_{17}	1077	0.32	0.26	0.11	0.15	0.17	0.05
ν_{16}	1128	1.60	0.55	0.53	1.47	0.50	0.43
ν_{14}	1278	0.79	0.34	0.23	0.71	0.30	0.18
ν_{13}	1362	0.15	0.04	0.04	0.18	0.05	0.04
ν_{12}	1393	0.92	0.34	0.25	1.98	0.47	0.46
ν_8	1522	1.01	0.33	0.25	0.88	0.28	0.19
ν_7	1545	0.48	0.22	0.12	2.24	0.45	0.47

energy in acetonitrile appears in ν_{20} and ν_{16}, this indicates that the short-time structural dynamics is significantly along the complex C5N4C6 symmetry stretch and C1C2+C1S3+C1N4 stretch reaction coordinates based on their normal mode displacements. The structural changes along the C1C2+C1S3+C1N4 coordinates consist well with the major $\pi_{H-1}\rightarrow\pi^*_L$ electronic transition of S_3 state that weakens the C=S and C=N bonds and strengthens the C−C bond. However, the large structural change along the C5N4C6 symmetry stretch coordinate is hardly explained by the major $\pi_{H-1}\rightarrow\pi^*_L$ electronic transition since it does not lead to the large variation of the electronic density in the C5−N4−C6 bond.

The intensity of the ν_{16} mode relative to that of the ν_{20} mode decreases as the laser line goes from 239.5 nm to 273.9 nm. The intense intensity of the ν_{16} mode in the 239.5 nm resonance Raman spectrum in acetonitrile can be explained by the major $n_H\rightarrow Ryd_3$ transition of the B-band absorption that makes the electronic density around H10, H11, and S atoms change greatly so that significant motions of the C1S3 bend+C5-methyl wag are expected to occur in the Franck-Condon region of the S_5 state. However the moderate intensity of the ν_{16} mode in the 273.9 nm resonance Raman spectrum is hardly explained by the electronic transitions of the A-band absorption. This suggests that the appearance of the moderate intensity of the ν_{16} mode in the 273.9 nm resonance Raman spectrum is likely due to a significant vibronic-coupling between the S_3 and S_5 states. The significant intensity of the combination band $\nu_{20}+\nu_{16}$ in different laser excitations further suggests that the S_3-S_5 vibronic-coupling exists in the wide range of energy. The preresonance enhancement of the weak B-band absorption is not considered as a major source of the significant intensity of the ν_{16} mode in the A-band resonance Raman spectra since it usually enhances the fundamental modes but not the overtones and combination bands. For similar reason, the variation in the intensity of the ν_{14} mode relative to that of the ν_{20} mode also suggests that there exists the S_3-S_5 vibronic-coupling.

DOI:10.1063/1674-0068/28/cjcp1409152

Figure 6 shows that the intensity pattern of the A-band resonance Raman spectra of DMTAA in acetonitrile differs significantly from that in water. The most important difference lies in the intensity variation of ν_7 and ν_{12} relative to that of ν_{20}. According to Fig.6 and Table III, the vibrational reorganizational energies partitioned in the ν_7 and ν_{12} modes in water are about 3.9 and 1.8 times those in acetonitrile respectively. The increased intensity of ν_7 and ν_{12} in water suggests that more available energy is partitioned into the degree of freedom of the H10C5H11 scissor/C1N4 stretch/N4C6H13 bend/C6-methyl umbrella vibrations, while the decreased intensity of ν_{16} in water suggests that less available energy is distributed among the degree of freedom of the C1C2 stretch/C1S3 bend/C5-methyl wag vibrations when compared to that in acetonitrile. The intensity of overtone $2\nu_7$ is about 3 times stronger than that of $2\nu_{20}$ and that of $\nu_7+\nu_{12}$ is much intenser than that of $\nu_{20}+\nu_{12}$, *etc.* indicating that the structural dynamics along the H10C5H11 scissor+C1N4 stretch+N4C6H13 bend reaction coordinates in S_3 state undergo larger normal mode displacements in water than in acetonitrile.

The weak C1 out-of-plane bend+C2-methyl twist mode ν_{34} in the A″ irreducible representation is observed in the 309.1 nm resonance Raman spectrum of DMTAA in water. This indicates that the Herzberg-Teller vibronic-coupling mechanism [24, 25] and/or the Franck-Condon region CI mechanism [12−14] work for the spectrum. Figure 7 displays the CASSCF computed geometric structures of $S_{1,min}$ and $S_{2,min}$ as well as S_3/S_1 conical intersection point. The excitation energy for $S_{2,min}$ is 140 kcal/mol, which is too high for 309.1 nm wavelength to reach, and this result, together with the C_s symmetry nature of the $S_{2,min}$ structure, suggests that the activation of ν_{34} is not due to the structural dynamics towards $S_{2,min}$ structure. The 309.1 nm excitation is energetically between those of $S_{1,min}$ and CI(S_3/S_1), and this suggests that it is possible that 309.1 nm probes the structural dynamics initiated from CI(S_3/S_1) to $S_{1,min}$, just as the revelation [13], previously found for the structural dynamics of 4-cyanobenzaldehyde in the light absorbing $S_2(\pi\pi^*)$ state, that the resonance Raman intensity pattern in the preresonance region signs mainly the structural dynamics along the portion of potential energy surface initiating from CI[$S_1(n\pi^*)/S_2(\pi\pi^*)$] point to somewhere of the $S_1(n\pi^*)$ state. The appearance of the C1 out-of-plane bend+C2-methyl twist ν_{34} mode of DMTAA correlates well with the prominent differences in the orientation of C2-methyl group and the dihedral ($D_{S_{1,min}(C2-C1-N4-C6)}=-150.5°$, $D_{S_2/S_1(C2-C1-N4-C6)}=179.6°$) between the structures of $S_{1,min}$ and CI(S_3/S_1), and this indicates that the $S_{1,min}$ species forms via a ultrafast CI(S_3/S_1) channel upon the molecule is populated to the $S_3(\pi\pi^*)$ state. The major decay channel is proposed to be from $S_{3,FC}(\pi\pi^*)\rightarrow S_3(\pi\pi^*)/S_{31}(n\pi^*)\rightarrow S_1(n\pi^*)$.

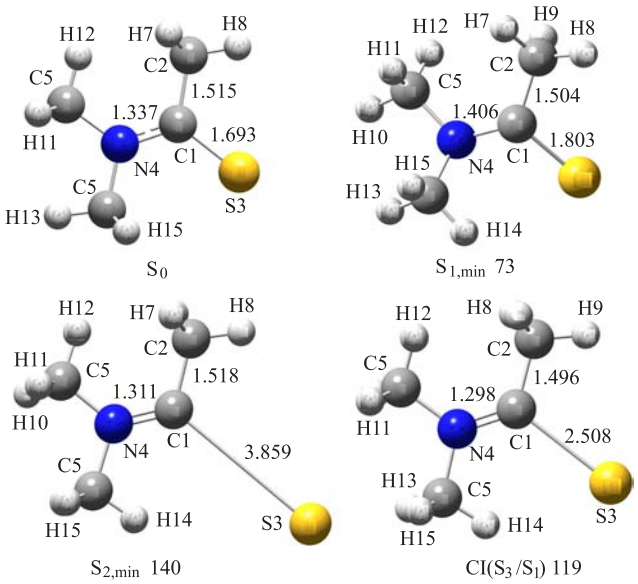

FIG. 7 Schematic diagram of the geometry structures of the lower-lying singlet and triplet excited states, the conical intersection and intersystem crossing points computed at the CASSCF(6,5)/6-31G(d) level of theory. The excitation energy are also give in kcal/mol.

Further work is thus required to deeply understand the short-time structural dynamics of DMTAA in different solvents. The present work indicates the normal mode displacements in S_3 state are solvent-dependent, but the detail mechanism is presently unclear, and we try to quantitatively determine the normal mode displacements by using the time-dependent wave-packet theory and the subsequent conversion to the internal coordinate displacement at different time in femtosecond timescale [20, 26, 27]. This would allow us to get the exact bond length and bond angle changes within a few tens fs. Hydrogen bonding interaction may be a good point of penetration to gain insight into the mechanism buried behind the A-band resonance Raman spectra. We also try the CASSCF and time-dependent density functional theory calculations to explore the excited state hydrogen bonding interactions at different active sites. This, together with the results of the time-dependent wave-packet theory modeling, will provide us a clearer picture about the nature of the short-time structural dynamics of DMTAA in different solvents.

IV. CONCLUSION

Focused on the excited state deactivation path of DMTAA, the vibrational spectra and the excited state structural dynamics in Franck-Condon region are studied by using the resonance Raman spectroscopy and quantum mechanical calculations. Most of the A-band resonance Raman intensities of DMTAA in acetonitrile and water can be assigned to the fundamen-

DOI:10.1063/1674-0068/28/cjcp1409152

tals, overtones and combination bands of about ten Franck-Condon modes: ν_7, ν_8, ν_{12}, ν_{13}, ν_{14}, ν_{15}, ν_{16}, ν_{17}, ν_{19}, ν_{20}. The structural changes along the C1C2+C1S3+C1N4 coordinates as predicted by the A-band resonance Raman intensity pattern consist well with the major $\pi_{H-1}\rightarrow\pi_L^*$ electronic transition that weakens the C=S and C=N bonds and strengthens the C−C bond as revealed by CASSCF and DFT calculations. The significant intensity of the combination band $\nu_{20}+\nu_{16}$ in different laser excitations suggests that the S3−S5 vibronic-coupling exists in the wide range of energy. The variation in the intensity of the ν_{14} mode relative to that of the ν_{20} mode can be interpreted as the existence of the S3−S4 vibronic-coupling. The appearance of the C1 out-of-plane bend+C2-methyl twist ν_{34} mode in the 309.1 nm resonance Raman spectrum does not correlate to the structural dynamics towards $S_{2,min}$ structure, but correlates well with the prominent differences in the orientation of C2-methyl group and the dihedral ($D_{S_{1,min}(C2-C1-N4-C6)}$=−150.5°, $D_{S_2/S_1(C2-C1-N4-C6)}$=179.6°) between the structures of $S_{1,min}$ and CI(S_3/S_1). It indicates that the $S_{1,min}$ species forms from $S_{3,FC}$ via a ultrafast CI(S_3/S_1) channel. The major decay channel is revealed from $S_{3,FC}(\pi\pi^*)\rightarrow S_3(\pi\pi^*)/S_1(n\pi^*)\rightarrow S_1(n\pi^*)$.

V. ACKNOWLEDGMENTS

This work was supported by the National Natural Science Foundation of China (No.21033002 and No.21202032) and the National Basic Research Program of China (No.2013CB834604).

[1] A. Maciejewski and R. P. Steer, Chem. Rev. **93**, 67 (1993).
[2] H. Rostkowska, L. Lapinski, A. Khvorostov, and M. J. Nowak, J. Chem. Phys. A **107**, 6373 (2003).
[3] L. Lapinski, H. Rostkowska, A. Khvorostov, and M. J. Nowak, Phys. Chem. Chem. Phys. **5**, 1524 (2003).
[4] R. Knudsen and Y. Hase, J. Mol. Struc. **321**, 197 (1994).
[5] S. Dapprich and G. Frenking, Chem. Phys. Lett. **205**, 337 (1993).
[6] M. J. Nowak, L. Lapinski, H. Rostkowska, A. Les, and L. Adamowicz, J. Phys. Chem. **94**, 7406 (1990).
[7] M. J. Nowak, L. Lapinski, H. Rostkowska, A. Les, and L. Adamowicz, J. Phys. Chem. **95**, 2404 (1991).
[8] D. Prusinowska, L. Lapinski, M. J. Nowak, and L. Adamowicz, Spectrochim. Acta **51A**, 1809 (1995).
[9] H. Rostkowska, L. Lapinski, and M. J. Nowak, J. Phys. Chem. A **107**, 804 (2003).
[10] H. Rostkowska, L. Lapinski, I. Reva, B. J. Almeida, M. J. Nowak, and R. Fausto, J. Phys. Chem. A **115**, 12142 (2011).
[11] G. J. Zhao and K. L. Han, Acc. Chem. Res. **45**, 404 (2012).
[12] X. F. Wu, X. M. Zheng, H. G. Wang, Y. Y. Zhao, X. G. Guan, and D. L. Phillips, J. Chem. Phys. **133**, 134507 (2010).
[13] Y. Yang, S. Pan, J. D. Xue, X. M. Zheng, W. H. Fang, and D. L. Phillips, J. Raman Spectrosc. **45**, 105 (2014).
[14] J. L. Guo, C. Liu, B. B. Xie, Y. Y. Zhao, K. M. Pei, H. G. Wang, and X. M. Zheng, J. Raman Spectrosc. **43**, 1477 (2012).
[15] J. W. Jian, H. B. Zhang, C. Q. Chen, Y. Y. Zhao, and X. M. Zheng, J. Raman Spectrosc. **44**, 582 (2013).
[16] X. L. Jiang, K. M. Pei, H. G. Wang, X. M. Zheng, W. H. Fang, and D. L. Phillips, J. Phys. Chem. A **111**, 13182 (2007).
[17] Y. Q. Wang, H. G. Wang, S. Q. Zhang, K. M. Pei, X. M. Zheng, and D. L. Phillips, J. Chem. Phys. **125**, 214506 (2006).
[18] R. Du, C. Liu, Y. Y. Zhao, K. M. Pei, H. G. Wang, X. M. Zheng, M. D. Li, J. D. Xue, and D. L. Phillips, J. Phys. Chem. B **115**, 8266 (2011).
[19] X. M. Zheng, Y. L. Li, and D. L. Phillips, J. Phys. Chem. A **108**, 8032 (2004).
[20] A. B. Myers and T. R. Rizzo, *Laser Techniques in Chemistry*, New York: Wiley, 325 (1995).
[21] A. B. Myers, B. Li, and X. Ci, J. Chem. Phys. **89**, 1876 (1988).
[22] R. Ouillon and S. Adam, J. Raman Spectrosc. **12**, 281 (1982).
[23] M. J. Frisch, G. W. Trucks, H. B. Schlegel, G. E. Scuseria, M. A. Robb, J. R. Cheeseman, J. A. Jr. Montgomery, T. Vreven, K. N. Kudin, J. C. Burant, J. M. Millam, S. S. Iyengar, J. Tomasi, V. Barone, B. Mennucci, M. Cossi, G. Scalmani, N. Rega, G. A. Petersson, H. Nakatsuji, M. Hada, M. Ehara, K. Toyota, R. Fukuda, J. Hasegawa, M. Ishida, T. Nakajima, Y. Honda, O. Kitao, H. Nakai, M. Klene, X. Li, J. E. Knox, H. P. Hratchian, J. B. Cross, C. Adamo, J. Jaramillo, R. Gomperts, R. E. Stratmann, O. Yazyev, A. J. Austin, R. Cammi, C. Pomelli, J. W. Ochterski, P. Y. Ayala, K. Morokuma, G. A. Voth, P. Salvador, J. J. Dannenberg, V. G. Zakrzewski, S. Dapprich, A. D. Daniels, M. C. Strain, Ö. Farkas, D. K. Malick, A. D. Rabuck, K. Raghavachari, J. B. Foresman, J. V. Ortiz, Q. Cui, A. G. Baboul, S. Clifford, J. Cioslowski, B. B. Stefanov, G. Lui, A. Liashenko, P. Piskorz, I. Komaromi, R. L. Martin, D. J. Fox, T. Keith, M. A. Al-Laham, C. Y. Peng, A. Nanayakkara, M. Challacombe, P. M. W. Gill, B. Johnson, W. Chen, M. W. Wong, C. Gonzalez, and J. A. Pople. *Gaussian 03, Revision B.02*, Pittsburgh, PA: Gaussian Inc, (2003).
[24] H. G. Wang, J. Xu, J. M. Wan, Y. Y. Zhao, and X. M. Zheng, J. Phys. Chem. B **114**, 3623 (2010).
[25] D. J. Swanton, G. B. Bacskay, and N. S. Hush, Chem. Phys. **83**, 69 (1984).
[26] D. M. Chen, T. He, D. F. Cong, Y. H. Zhang, and F. C. Liu, J. Phys. Chem. A **105**, 3981 (2001).
[27] X. Zheng and D. L. Phillips, J. Chem. Phys. **108**, 5772 (1998).

DOI:10.1063/1674-0068/28/cjcp1409152